CD59-Regulated Ras Compartmentalization Orchestrates Antitumor T-cell Immunity

Luying Li[1], Peipei Ding[1], Xinyue Lv[1], Suhong Xie[2], Ling Li[1], Jianfeng Chen[1], Danlei Zhou[1], Xiaochao Wang[1], Qi Wang[1], Wei Zhang[1], Yanqing Xu[1], Renquan Lu[2], and Weiguo Hu[1,3]

ABSTRACT

T cell–mediated immunotherapy represents a promising strategy for cancer treatment; however, it has achieved satisfactory clinical responses in only a limited population. Thus, a broader view of the T-cell immune response is required. The Ras/MAPK pathway operates in many important signaling cascades and regulates multiple cellular activities, including T-cell development, proliferation, and function. Herein, we found that the typical membrane-bound complement regulatory protein CD59 is located intracellularly in T cells and that the intracellular form is increased in the T cells of patients with cancer. When intracellular CD59 is abundant, it facilitates Ras transport to the inner plasma membrane via direct interaction; in contrast, when CD59 is insufficient or deficient, Ras is arrested in the Golgi, thus enhancing Ras/MAPK signaling and T-cell activation, proliferation, and function. *mCd59ab* deficiency almost completely abolished tumor growth and metastasis in tumor-bearing mice, in which $CD4^+$ and $CD8^+$ T cells were significantly increased compared with their proportions in wild-type littermates, and their proportions were inversely correlated with tumor growth. Using bone marrow transplantation and $CD4^+$ and $CD8^+$ T-cell depletion assays, we further demonstrated the critical roles of these cells in the potent antitumor activity induced by *mCd59ab* deficiency. Reducing CD59 expression also enhanced MAPK signaling and T-cell activation in human T cells. Therefore, the subcellular compartmentalization of Ras regulated by intracellular CD59 provides spatial selectivity for T-cell activation and a potential T cell–mediated immunotherapeutic strategy.

Introduction

Immunotherapy, in which T lymphocytes play a cornerstone role, is becoming an effective therapeutic strategy for various types of cancer. To potentiate the antitumor T-cell response, antibodies against immune checkpoint molecules, such as CTLA4 and programmed cell death protein 1 (PD-1)/programmed death-ligand 1 (PD-L1), have achieved remarkable clinical responses, albeit in only a minority of patients and indications (1). In their immunosuppressive roles, CTLA4 suppresses T-cell receptor (TCR) signaling by competing with CD28 for CD80 and CD86 due to its higher avidity and affinity (2), and PD-1 directly transmits a negative costimulatory signal to dampen T-cell activation through interactions with PD-L1 and PD-L2 (3). In addition, genetically engineered T cells, such as chimeric antigen receptor (CAR) T cells, have demonstrated remarkable potency, although mainly in hematologic malignancies, especially B-cell malignancies (4). However, CAR T-cell therapeutics display limited efficacy against solid tumors due to, at least in part, the immunosuppressive effects of the tumor microenvironment. Thus, these unmet clinical needs require a broader view of T-cell immunity for the rational design of next-generation immunotherapies.

Ras proteins are small GTPase molecular switches that are essential for T-cell proliferation, development, and function (5). There are three major isoforms, H-, K-, and N-Ras, which are 95% identical in the N-terminus, whereas the C-terminal hypervariable region (HVR) is much more dissimilar. N-Ras is preferentially activated downstream of TCR signaling, whereas H-Ras is expressed much lower than the K-Ras and N-Ras isoforms (6). The C-terminal HVR guides the posttranslational modification and membrane interaction of the primary *Ras* gene products, thereby directing their different subcellular localizations, trafficking and functions at the inner plasma membrane and endomembranes [membranes of endosome, endoplasmic reticulum (ER), Golgi, and mitochondria; ref. 7]. Ras signaling at the Golgi is mediated by RasGRP1 (8) and PLCγ (9), whereas signaling at the ER involves RasGRFs (10). In addition, Ras activation is rapid and transient in the plasma membrane but delayed and sustained at the Golgi (11, 12). Therefore, the subcellular compartmentalization of Ras proteins may underlie their biological differences in the complexity of the signaling output (13).

The complement system is a central component of innate immunity and enhances the adaptive immune response. Complement activation may lead to the assembly of the membrane attack complex (MAC) in the cell membrane, which can be specifically blocked by CD59, a membrane-bound complement regulatory protein (14). CD59 in autologous cells can protect from deleterious complement attack; however, CD59 in tumor cells can be hijacked to evade complement-based immune surveillance (15, 16). CD59 also plays a complement-independent role in signal transduction. We previously demonstrated that CD59 deficiency in esophageal cancer cells induced radiosensitivity by suppressing the phosphorylation of Src at Y416 (17). It also has intracellular functions, such as involvement in stimulating insulin secretion from pancreatic β cells (18, 19). Most CD59 protein in pancreatic β cells is located intracellularly. The removal of cell surface-bound CD59 with phospholipase C had no effect on insulin secretion, whereas downregulating intracellular CD59 markedly decreased the ability of β cells to secrete insulin, suggesting that intracellular CD59 was especially

[1]Fudan University Shanghai Cancer Center and Institutes of Biomedical Sciences, Shanghai Medical College, Fudan University, Shanghai, China. [2]Department of Clinical Laboratory, Fudan University Shanghai Cancer Center, Fudan University, Shanghai, China. [3]Key Laboratory of Breast Cancer in Shanghai, Fudan University Shanghai Cancer Center, Fudan University, Shanghai, China.

Corresponding Author: Weiguo Hu, Cancer Institute, Fudan University Shanghai Cancer Center, 270 Dong'an Road, Shanghai 200032, China. Phone: 213-477-7590; Fax: 216-417-2585; E-mail: weiguohu@fudan.edu.cn

Cancer Immunol Res 2022;10:1475–89

doi: 10.1158/2326-6066.CIR-21-1072

involved in insulin release (18). Mechanistically, endogenous non–glycosylphosphatidylinositol (GPI)-anchored CD59 splice variants in human pancreatic islets interact with the SNARE proteins VAMP2 and SNAP25 and rescue insulin secretion in CD59-knockout cells (20). In addition, it has been reported that T-cell activation is associated with CD59 through its membrane-bound form. Anti-CD59, together with appropriate costimulation, can increase cytoplasmic free Ca^{2+}, thus inducing IL2 production and T-cell proliferation (21). CD59 may bind to CD2 as a CD2 accessory molecule (22); however, this interaction is questioned by some studies (23, 24), and T-cell costimulation by CD59 is dependent on the expression of CD58 (25). The virus-specific $CD4^+$ T-cell response in *mCd59a*-deficient mice was found to be significantly enhanced, which was independent of complement activation and required the presence of antigen-presenting cells (APC) (26). Downregulation of CD59 in $CD4^+$ T cells was observed only when APCs were present in a proliferation experiment, in which an unidentified ligand expressed on the APC surface bound to CD59 on $CD4^+$ T cells, thus resulting in transmission of negative signals to the responding T cells (27, 28). Tyrosine-protein kinase LCK mediates signal transmission from CD59 to the TCR/CD3 pathways in Jurkat T cells, suggesting that CD59 may modulate T-cell responses through LCK (29). However, the mechanism by which CD59, especially its intracellular form, modulates T-cell functions remains largely elusive.

In the current study, we revealed that by interacting with Ras proteins, CD59 regulates Ras subcellular compartmentalization to the plasma membrane or Golgi to modify T-cell activation by regulating MAPK signaling downstream of Ras, which was also verified in *mCd59ab*-deficient mice and human T cells, thus regulating tumor progression.

Materials and Methods

Cell culture

Murine TC-1 cells, Jurkat T cells, and HEK293T cells were purchased from Cell Bank/Stem Cell Bank, Chinese Academy of Sciences (Shanghai) from 2015 to 2018, and passages between 5 and 20 were used after initial revival from frozen stocks. These cells were authenticated using the short tandem repeat assay. Murine TC-1 cells, Jurkat T cells were cultured in RPMI1640 medium (SH30809.01, Hyclone, South Logan, UT), and HEK293T cells were cultured in DMEM (SH30243.01, Hyclone, South Logan, UT) at 37°C in humidified incubators containing 5% CO_2. Both culture media were supplemented with 10% FBS (10270106, Gibco, Thermo Fisher Scientific, Waltham, MA) and 1% penicillin/streptomycin (S110JV, Basaimedia, Shanghai, China). All cell lines were routinely tested to ensure there was no *Mycoplasma* contamination with One-step Quickcolor Mycoplasma Detection Kit (MD001, Shanghai Yise Medical Technology, Shanghai, China).

Human blood samples

Blood was collected from 26 patients with colorectal cancer, 25 patients with lung cancer and 18 healthy volunteers for detection of CD59 in T cells after written informed consent form was provided. Patients who were not subjected to any surgical resection or systemic treatment were included (Supplementary Data 1, 2). The harvested peripheral blood mononuclear cells (PBMC) were stored in liquid nitrogen for later use. This study was approved by the ethics committee of the Fudan University Shanghai Cancer Center (ethics number 050432–4-1805C) and was conducted according to Declaration of Helsinki principles.

Mice

Wild-type (WT) C57BL/6 mice were purchased from Shanghai SLAC Laboratory Animal Co., Ltd. (Shanghai, China). *mCd59ab*-deficient mice were backcrossed onto the C57BL/6 genetic background for at least nine generations (30). Age-matched 8- to 10-week-old male mice were employed for related experiments. All experiments were conducted in a blinded manner. All mice were raised in the animal facility of Shanghai Medical School, Fudan University under specific pathogen-free conditions. All animal experiments and care were performed with the consent of the Animal Ethics Committee at Shanghai Medical School, Fudan University (ethics number 2019 cancer center JS-032), and complied with the Guide for the Care and Use of Laboratory Animals published by the US NIH.

Antibodies and reagents

The commercial antibodies used in this study are listed in Supplementary Table S1. The MEK1/2 kinase inhibitor U0126 (HY-12031) and JNK kinase inhibitor JNK-IN-8 (HY-13319) were purchased from MedChemExpress (Monmouth Junction, NJ). The p38 kinase inhibitor SB203580 (S1076) was obtained from Selleck Chemicals (Shanghai, China).

Plasmid construction and lentivirus production

To construct the RNAi plasmid, the short hairpin RNA (shRNA) sequences specific for CD59, N-Ras, K-Ras, and H-Ras were inserted into the pLKO.1-puro (10878, Addgene, Watertown, MA) or pLKO.1-EGFP (an EGFP sequence in place of the puro sequence) vector. The pLKO.1 plasmid was transfected into 293T cells with the envelope plasmid PMD2.G (12259, Addgene, Watertown, MA) and the packaging plasmid psPAX2 (12260, Addgene, Watertown, MA) with DNA transfection reagent (TF201201, Neofect Biotech, Beijing, China) to generate lentiviruses. The viral supernatants were harvested after 48 hours or 72 hours of transfection and filtered through a 0.45-μm syringe to concentrate the viruses 50-fold with polyethylene glycol 8000 (PEG 8000; Diamond, Shanghai, China). The CD59, N-Ras, K-Ras, and H-Ras specific shRNA sequences used are listed in Supplementary Table S2.

Lentiviral transduction

Human PBMCs were isolated from 3 or 4 healthy donors' blood samples via gradient centrifugation with Lymphoprep (07851/07861, StemCell, Vancouver, BC, Canada) and used immediately for experiments. Informed consent was obtained from healthy donors. This study was approved by the ethics committee of the Fudan University Shanghai Cancer Center (ethics number 050432–4-1805C) and was conducted according to Declaration of Helsinki principles. Human T cells were stimulated with Dynabeads human T-Activator CD3/CD28 (11132D, Gibco, Waltham, MA) at a bead-to-cell ratio of 1:1 for 48 hours. Then, the activated T cells were transduced with a lentivirus (multiplicity of infection = 6) on RetroNectin (5 μg/mL; T100A, Takara, Tokyo, Japan)-precoated 24-well plates in the presence of polybrene (5 μg/mL) (sc-134220, Santa Cruz, CA) for 24 hours. Infection was carried out by centrifugation at 1,200 *g* for 1 hour. The infected T cells were cultured at a density of 0.5×10^6 to 2×10^6 cells/mL in X-VIVO 15 medium (04–418Q, Lonza, Basel, Switzerland) supplemented with 5% human AB serum (100–512, Gemini Bio-products, Broderick, CA) in the presence of recombinant human IL2 (200 U/mL; AF-200–02, PeproTech, Rocky Hill, NJ) and 1% penicillin/streptomycin. The transduced human T cells (pLKO.1-shNC-EGFP or pLKO.1-shCD59-EGFP) were expanded for at least 7 days prior to being used in subsequent assays. The transduction efficiency was

determined by FACS analysis of EGFP expression. Jurkat T cells were transduced with the pLKO.1-shNC-puro or pLKO.1-shCD59-puro lentivirus for 48 hours and then selected with puromycin at a concentration of 6 μg/mL. Jurkat-shCD59 cells were transduced with the pLKO.1-shN-, K-, and H-Ras lentivirus for 48 hours and then conducted the follow-up experiments.

Naïve mouse $CD4^+$/$CD8^+$ T-cell isolation and stimulation

Naïve mouse $CD4^+$/$CD8^+$ T cells were purified from spleens following the manufacturer's instructions of a mojoSort mouse $CD4^+$/$CD8^+$ T-cell isolation kit ($CD4^+$ T-cell isolation kit, 480033; $CD8^+$ T-cell isolation kit, 480008; BioLegend, San Diego, CA), and the purity was confirmed by FACS. The purities of $CD4^+$ and $CD8^+$ T cells were both greater than 90%. These cells (1×10^6 cells/mL) were activated with plate-bound anti-mouse CD3/CD28 antibodies (anti-mouse CD3, 100340; anti-mouse CD28, 102112; 2 μg/mL each, BioLegend, San Diego, CA) and cultured in RPMI1640 medium supplemented with mIL2 (100 U/mL, 212–12, PeproTech, Rocky Hill, NJ) and 10% FBS for the indicated times. Cells were harvested at the indicated time for surface staining and restimulated for 4 to 6 hours for intracellular cytokine staining. For CFSE (423801, BioLegend San Diego, CA) labeling, isolated $CD4^+$/$CD8^+$ T cells (1×10^7 to 10×10^7 cells/mL) were stained with 5 μmol/L CFSE.

Flow cytometry

For leukocyte immunostaining, the fixable viability dye eFluor 780 (25200072, eBioscience, San Diego, CA) was used to irreversibly label dead cells prior to surface staining at 1 μL/mL for 1×10^6 to 10×10^6 cells/mL in PBS. Then, the samples were incubated with anti-CD16/32 monoclonal antibodies (mAb) in a 1% BSA/PBS solution for 15 minutes on ice to block nonspecific Fc receptor binding. Antibodies against CD3, CD4, CD8, CD11b, Gr-1, F4/80, Ly-6C, Ly-6G, NK1.1, CD19, CD59, CD25, PD-1, CTLA4, TIM-3, LAG3, C5b-9, and CD69 were used for surface staining according to the manufacturer's instructions.

For intracellular staining of IL2, IFNγ, TNFα, perforin, and granzyme B, cells were stimulated with a cell activation cocktail (phorbol 12-myristate 13-acetate/ionomycin/brefeldin A, 423304, BioLegend, San Diego, CA) for 4 to 6 hours at 37°C following intracellular staining instructions. For Ki67 expression analysis, cells were fixed and permeabilized using a FoxP3 Fix/Perm kit (421403, BioLegend, San Diego, CA) according to the manufacturer's instructions and then stained with an anti-Ki67. For intracellular staining of p-ERK, p-p38, and p-JNK, cells were fixed (Fixation Buffer, 420801, BioLegend, San Diego, CA) and permeabilized (Intracellular Staining Perm Wash Buffer, 421002, BioLegend, San Diego, CA) according to the manufacturer's instructions. Cells were acquired on a BD FACSCanto II flow cytometer or Beckman Cytomics FC500, and data were analyzed with FlowJo software (TreeStar, Ashland, OR). Cells that were stained with an isotype control antibody and unstained cells were used as negative controls, and single-color–stained samples were used as compensation controls.

Mouse tumor models

Male *mCD59ab*$^{-/-}$ mice or WT littermates were injected subcutaneously in the left flank with TC-1 cells (2×10^5 cells/mouse) mixed at a 1:1 ratio with Matrigel (356234, Corning, NY). Beginning 1 week after cell injection, tumor size was measured every 2 to 3 days with Vernier calipers, and tumor volume was calculated using the following formula: volume (mm^3) = 0.5×longer diameter × (shorter diameter)^2. The maximal tumor diameter was restricted to 2 cm. Spleens and tumors were harvested, measured and photographed for related figures.

For the liver metastasis model, mice were anesthetized by isoflurane. Then using microdissection scissors, an 8-mm left flank incision in the left subcostal region was made, and the spleen was exposed. TC-1 cancer cells (4×10^6/mouse), which were suspended in 80-μL PBS, were injected into the distal tip of the spleen using a 27-gauge needle. To prevent the leakage of tumor cells from the spleen, we applied pressure to the pinhole injection site for 1 to 2 minutes with sterile cotton swabs before suturing the abdomen. The abdominal wall was closed with a 5–0 absorbable braided suture and the skin was closed using a 4–0 non-absorbable monofilament suture (31). When cachexia happened, mice were sacrificed, and the liver was examined for metastasis. Liver samples were fixed in 4% paraformaldehyde (G1101, Servicebio, Wuhan, China), embedded in paraffin and sectioned for hematoxylin and eosin (H&E) staining to examine metastases.

Bone marrow transplantation

WT or *mCD59ab*-deficient bone marrow (BM) was prepared from the femurs and tibias and suspended in PBS at a density of 1×10^8/mL. Recipient mice were injected intravenously with 1.5×10^7 BM cells from donor mice six hours after receiving 9.5 Gy irradiation. Four weeks later, the BM in the chimeric mice had reconstituted, and a subcutaneous tumor model could be established.

$CD4^+$/$CD8^+$ T-cell depletion

To deplete $CD4^+$ and/or $CD8^+$ T cells, mice were injected intraperitoneally with 150-μg anti-CD4 mAb (clone GK1.5, catalog no. BE0003–1, BioXCell, West Lebanon, NH), anti-CD8α mAb (clone 2.43, Cat. NO. BE0061, BioXCell, West Lebanon, NH), or rat IgG2b isotype control (clone LTF-2, catalog no. BE0090, BioXCell, West Lebanon, NH) 2 days before tumor inoculation and twice a week thereafter. $CD4^+$ and/or $CD8^+$ T-cell depletion was validated by FACS analysis of peripheral blood samples, showing a depletion efficiency of up to 99%.

qRT-PCR

Total RNA was extracted from cells with TRIzol reagent (10296010, Thermo Fisher Scientific, Waltham, MA). PrimeScript RT Master Mix (RR036A, Takara, Tokyo, Japan) was applied for reverse transcription, and 2-μg RNA was reverse transcribed into cDNA according to the manufacturer's instructions. Real-time PCR analysis of gene expression was conducted with SYBR Premix Ex Taq II (Tli RNaseH Plus; RR820Q, Takara, Tokyo, Japan) on a QuantStudio7 Flex Real-Time PCR System platform (Thermo Fisher Scientific) following the manufacturer's instructions. Gene expression was normalized to β-actin, a reference gene, and data were analyzed with QuantStudio Real-Time PCR Software (three biological and technical replicates for each sample). Data are presented as the fold change calculated by the $2^{-\Delta\Delta Ct}$ method. The primers used for qPCR are listed in Supplementary Table S3.

Coimmunoprecipitation, immunoblot, and mass spectrometry

For the coimmunoprecipitation (co-IP) experiment, cells were harvested as follows: cells were lysed with NP40 lysis buffer (P0013F, Beyotime, Shanghai, China), 10% glycerol, a phosphorylated protease inhibitor cocktail (B15001, Bimake, Houston, TX) and a protease inhibitor cocktail (B14001, Bimake, Houston, TX) for 1 hour on ice and then centrifuged for 30 minutes at 12,000 r.p.m. at 4°C. Ten percent of each supernatant was harvested as the input for Western blotting, and the remaining cell lysate was incubated with specific

antibodies at 4°C with continuous mixing overnight. Then, 50 μL protein A/G beads (B23202, Bimake, Houston, TX) was washed three times with lysis buffer and added to the supernatant mix for another 4 hours at 4°C. After removing the supernatant, the beads were washed 3 times with lysis buffer, boiled and resuspended in 50 μL 1x SDS loading buffer, and the immunoprecipitates were detected by silver staining or Western blotting. Equal amounts of total protein were electrophoresed by SDS-PAGE, followed by being transferred to polyvinylidene difluoride membranes. The membranes were blocked with 5% skim milk (A600669, Sangon Biotech, Shanghai, China) diluted with TBST and then incubated overnight at 4°C with primary antibodies (Supplementary Table S1). Secondary antibodies conjugated with HRP (SA00001, Proteintech, Chicago, IL) were added for 1 hour at room temperature and the protein bands were detected by using enhanced chemiluminescence reagent (SB-WB011, Sharebio, Shanghai, China). The images were captured with ImageQuant LAS 4000 Biomolecular Imager (GE Healthcare, Sunnyvale, CA). The specific silver-stained gel band was used for mass spectrometry analysis, and the data are shown in Supplementary Data 3 and Supplementary Data 4.

Immunocytochemistry assay

Jurkat T cells or $CD4^+$ and $CD8^+$ T cells of WT and *mCd59ab*-KO mice (4×10^4) were plated on coverslips and incubated for 30 minutes at 37°C, and then the remaining supernatant was removed. The cells were then fixed in 4% paraformaldehyde (G1101, Servicebio, Wuhan, China) for 20 minutes and permeabilized with 0.2% Triton X-100 (A110694, Sangon Biotech, Shanghai, China) in 1% BSA/PBS for 5 minutes. After 1 hour of blocking in 1% BSA (4240GR100, Biofroxx, Einhausen, Germany), the cells were incubated with primary anti-CD59 (1:200; ab9183, Abcam, Cambridge, MA), anti-Ras (1:200; ab108602 Abcam) and anti-Giantin (1:500; Gene Tex, San Diego, CA) overnight at 4°C and with fluorophore-conjugated secondary antibodies (1:1,000) for 1.5 hours at room temperature. Cell nuclei were stained with 4′,6-diamidino-2-phenylindole (DAPI; YEASEN, Shanghai, China). Fluorescence images were acquired with a Leica TCS-SP5 confocal system.

Statistical analysis

All data were analyzed with GraphPad Prism 7.0 (GraphPad Software, La Jolla, CA). All data was presented as the mean ± SEM or mean ± SD. Significance was evaluated with a two-tailed Student unpaired or paired *t* test. The significance of tumor volume changes was determined by two-way ANOVA. For correlation analysis, Pearson correlation coefficient test and Spearman rank correlation coefficient test were used. In all analyses, $P < 0.05$ was considered significant, and significance is presented as *, $P < 0.05$; **, $P < 0.01$; ***, $P < 0.001$; and ****, $P < 0.0001$.

Data availability

All data that support the findings of this study are available within the article and its Supplementary Data files or from the corresponding author upon reasonable request.

Results

Deficiency in *mCd59ab* impedes tumor growth and metastasis

CD59 is principally appreciated as a membrane-bound complement regulatory protein, but it is also reported to be located in the cytosol with an enigmatic complement-independent and/or immune-related

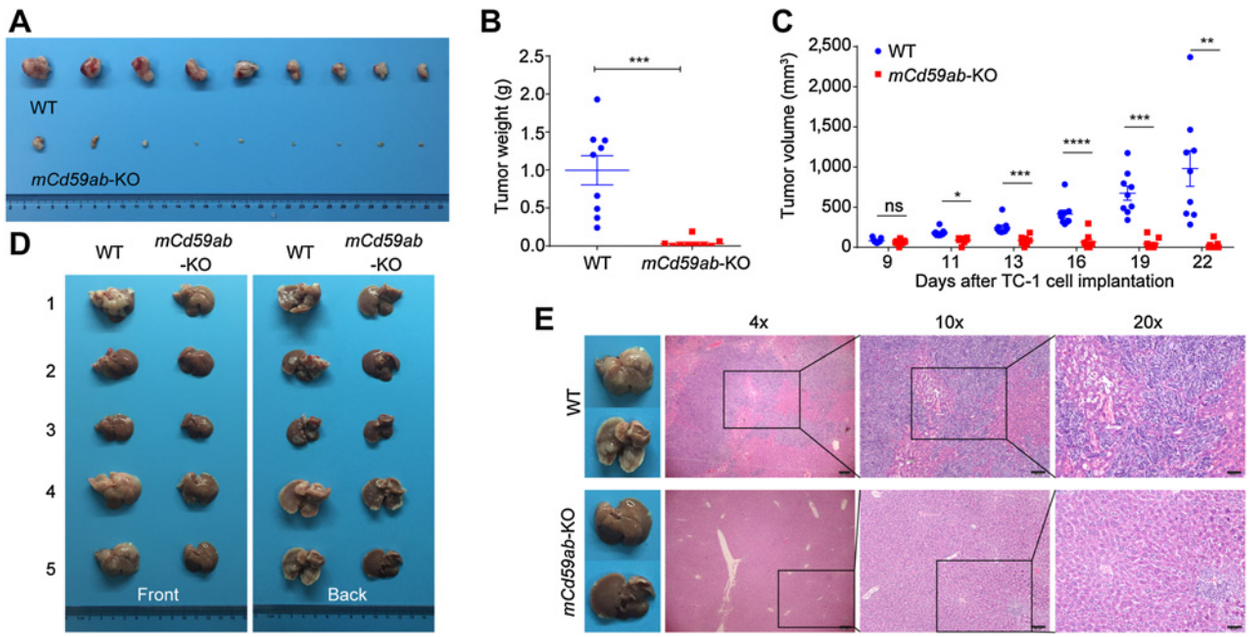

Figure 1.

mCd59ab deficiency prevents tumor growth and metastasis. **A–C,** WT and *mCd59ab*$^{-/-}$ littermates were injected subcutaneously with TC-1 cells and sacrificed on Day 22. Tumor growth was evaluated from a tumor image (**A**), tumor weight measurements (**B**) and tumor growth curves (**C**). $n = 9$/group. **D** and **E,** TC-1 cells were inoculated into the spleen to establish the hepatic metastasis model in WT and *mCd59ab*$^{-/-}$ littermates. Metastases are shown in liver images (**D**) and representative H&E-stained sections (**E**). Scale bar, 200 μm (4×); 100 μm (10×); and 50 μm (20×), $n = 5$/group. These experiments were performed twice, and data are expressed as the mean±SEM. The *P* values were determined by Student *t* test. *, $P < 0.05$; **, $P < 0.01$; ***, $P < 0.001$; ****, $P < 0.0001$.

function (17, 18), both of which indicate that *mCd59ab* deficiency may play an immune-associated role in tumor development. To explore CD59 function in tumor development, we monitored tumor growth and metastasis in *mCd59ab*-deficient mice. In humans, a single gene encodes CD59, whereas two *Cd59* genes are present in mice: *mCd59a* and *mCd59b*. Thus, WT and *mCd59ab*$^{-/-}$ (30) littermates were subcutaneously inoculated with mouse TC-1 lung cancer cells. We observed that tumor growth was almost completely inhibited in the *mCd59ab*-deficient mice compared with the WT littermates (**Fig. 1A–C**). Furthermore, we established a liver metastasis model by injecting TC-1 cells into the spleen and found widespread metastatic sites in the livers of WT mice compared with few visible metastases in *mCd59ab*$^{-/-}$ mouse livers (**Fig. 1D**), which was further confirmed by H&E staining (**Fig. 1E**). Together, these results demonstrate that *mCd59ab* deficiency dramatically impedes tumor growth and metastasis.

Cellular immune response in *mCd59ab*-deficient tumor-bearing mice

To understand the immune status of *mCd59ab*-deficient mice, we first compared the immune cell proportions in the spleen and blood of naïve WT and *mCd59ab*-deficient mice under physiologic conditions by flow cytometry. The results showed that there were no significant differences between WT and *mCd59ab*-deficient mice in the percentages of CD4$^+$ T cells, CD8$^+$ T cells, B cells, natural killer (NK) cells, myeloid-derived suppressor (MDSC)-like cells, macrophages, neutrophils, and monocytes in the spleen (Supplementary Fig. S1A) or blood (Supplementary Fig. S1B), suggesting that *mCd59ab* deficiency itself does not lead to complement-dependent cytolysis of immune cells other than nucleus-free erythrocytes (30) under physiologic conditions. More importantly, *mCD59ab* may exert a complement-independent function in the above tumor implantation model.

Next, using a similar protocol, we compared the proportions of these immune cells in the spleen and blood between the above WT and *mCd59ab*-deficient tumor-bearing mice. We observed that the proportions of splenic CD4$^+$ (**Fig. 2A**) and CD8$^+$ (**Fig. 2B**) T cells were elevated significantly in the *mCd59ab*-deficient tumor-bearing mice compared with the WT littermates and inversely correlated with tumor weight ($P < 0.0001$). However, the proportions of splenic MDSCs (**Fig. 2C**), neutrophils (**Fig. 2D**) and macrophages (**Fig. 2E**) were significantly lower in the *mCd59ab*-deficient tumor-bearing mice than in the WT littermates and positively correlated with tumor weight ($P < 0.001$).

The proportions of immune cells in the blood displayed a similar pattern to those in spleen, i.e., the percentages of CD4$^+$ (**Fig. 2F**) and CD8$^+$ (**Fig. 2G**) T cells were significantly higher, whereas MDSCs

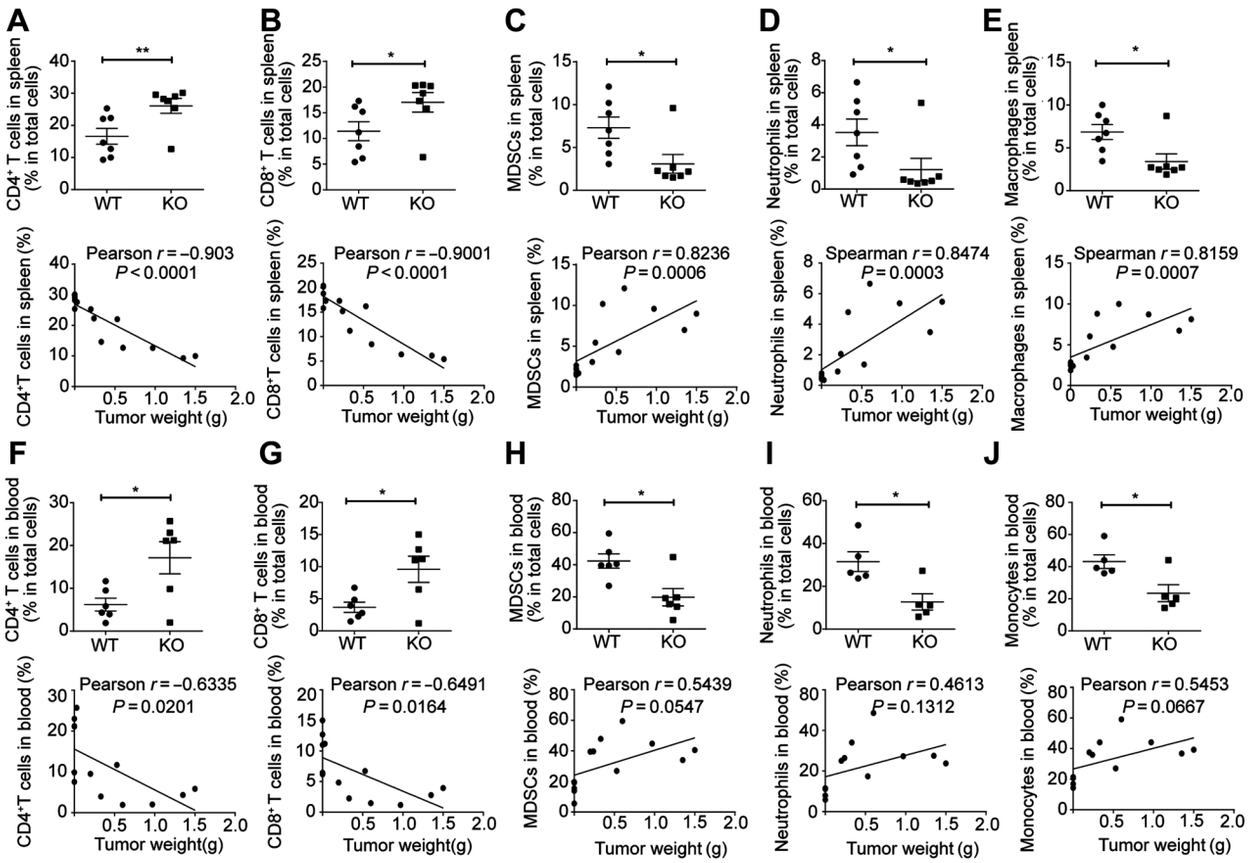

Figure 2.

The cellular immune response to tumor growth in WT and *mCD59ab*-deficient mice. Flow cytometry was used to detect immune cells in subcutaneously injected TC-1 tumor model on Day 22, and the correlations with tumor weight were further analyzed. **A–J,** The proportions of CD4$^+$ T cells (**A**, **F**), CD8$^+$ T cells (**B**, **G**), MDSCs (**C**, **H**), neutrophils (**D**, **I**), macrophages (**E**), and monocytes (**J**) in the spleen (**A–E**) and peripheral blood (**F–J**) were detected. Data are expressed as the mean±SEM; $n = 6\sim7$/group. The P values were determined by Student t test. *, $P < 0.05$; **, $P < 0.01$; ns, not significant.

(**Fig. 2H**), neutrophils (**Fig. 2I**) and monocytes (**Fig. 2J**) were significantly lower in *mCd59ab*-deficient tumor-bearing mice. However, the correlations between immune cell proportions in the blood and tumor weight were weaker than the splenic correlations. Although the proportions of blood $CD4^+$ (**Fig. 2F**) and $CD8^+$ (**Fig. 2G**) T cells were still inversely correlated with tumor weight ($P < 0.05$ in the blood vs. $P < 0.0001$ in the spleen), the proportions of MDSCs (**Fig. 2H**), neutrophils (**Fig. 2I**), and monocytes (**Fig. 2J**) in the blood had no significant correlation with tumor weight ($P > 0.05$), indicating that the immune cells in the spleen may be more relevant to tumor growth than those in the blood.

In addition, there were no differences between WT and *mCd59ab*-deficient tumor-bearing mice in B cells, NK cells and dendritic cells (DC) in the spleen (Supplementary Fig. S1C) or NK cells in the blood (Supplementary Fig. S1D), whereas we observed increased B cells in the blood of *mCd59ab*-deficient tumor-bearing mice (Supplementary Fig. S1E). The difference in frequency of some types of immune cells such as T lymphocytes was observed only in tumor bearing mice but not in naïve mice may result from the systemic immune response to the implanted tumor cells. Considering the important role of CD59 in restricting MAC formation during complement activation, we tested the MAC deposition in T cells derived from TC-1 tumor-bearing WT and *mCd59ab*$^{-/-}$ mice by FACS. The results showed that there was no significant differences in the deposition of MAC (C5b-9n) in blood $CD3^+$, $CD4^+$, and $CD8^+$ T cells of WT and *mCd59ab*$^{-/-}$ tumor-bearing mice (Supplementary Fig. S1F), which suggest that the CD59 deficiency-induced tumor suppression is complement independent.

Since myeloid cells could impact T-cell frequency and function, we analyzed the correlation between $CD4^+/CD8^+$ T-cell proportions and MDSC/neutrophil/macrophage/monocyte proportions in spleen and blood. The results demonstrated that $CD4^+/CD8^+$ T-cell proportions inversely correlated with MDSC/neutrophil/macrophage/monocyte proportions in spleen and blood, suggesting MDSCs/neutrophils/macrophages/monocytes might impair T-cell proliferation in this model (Supplementary Fig. S2).

Together, these results suggest that $CD4^+$ and $CD8^+$ T cells in the blood and especially in the spleen may be more relevant to tumor growth than MDSCs, neutrophils, macrophages and other immune cells, promoting the tumor-inhibitory effect of *mCd59ab* deficiency.

$CD4^+$ and especially $CD8^+$ T cells mediate the tumor-suppressive effect in *mCd59ab*-deficient mice

CD59 is widely expressed in most blood cells and a variety of tissues. To further clarify the origin of CD59 contributing to tumor progression, we generated chimeric mice by BM transplantation, and these mice were then subcutaneously inoculated with TC-1 tumor cells. The chimeric efficiency was confirmed by measuring mCd59a expression in blood cells from the indicated tumor-bearing mice (Supplementary

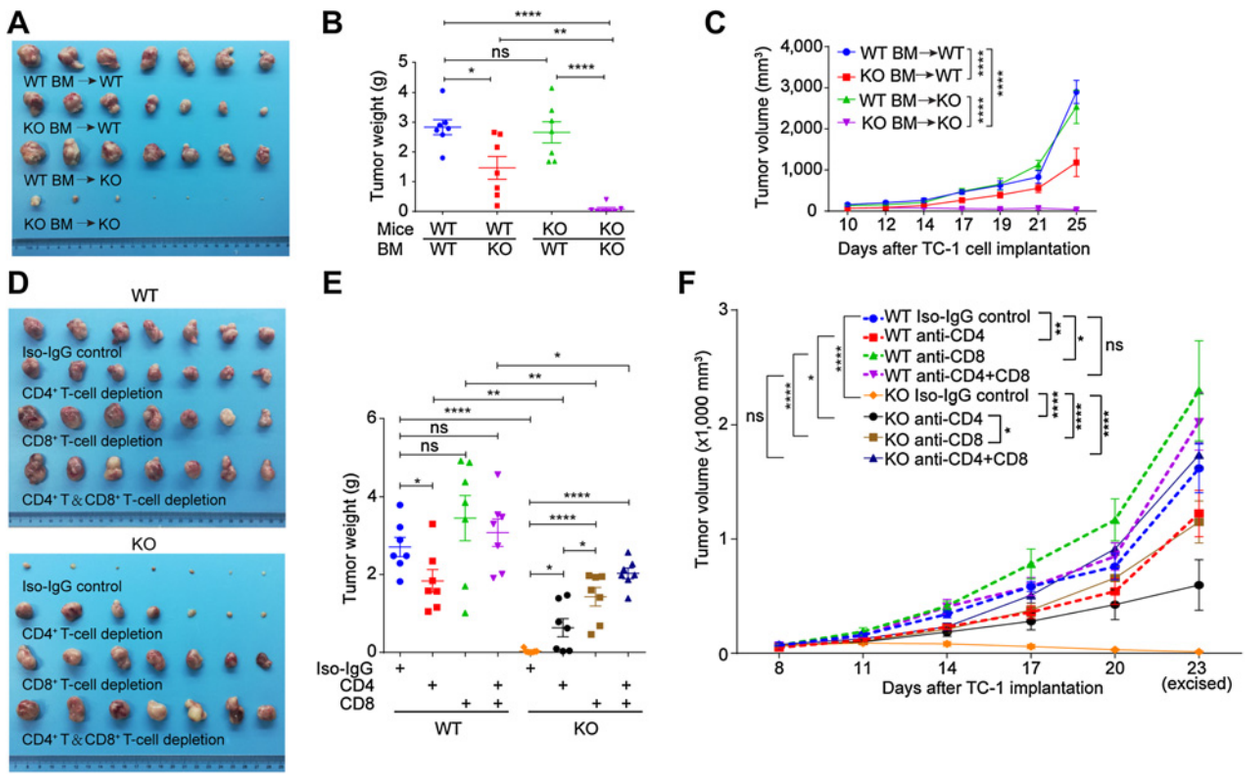

Figure 3.

$CD4^+$ and especially $CD8^+$ T cells determine the antitumor activity in *mCd59ab*-deficient mice. **A–C,** TC-1 cells were implanted subcutaneously in BM-transplanted chimeric mice, combinations of *mCd59ab*-WT or -KO donor and recipient, as indicated. Tumor image (**A**), tumor weight (**B**), and tumor growth curve (**C**). **D–F,** WT and *mCd59ab*$^{-/-}$ littermates were implanted subcutaneously with TC-1 cells and received $CD4^+$ or $CD8^+$ depleting IgG antibody treatments as indicated. Tumor image (**D**), tumor weight (**E**), and tumor growth curve (**F**). Data are expressed as the mean±SEM; $n = 7$/group; The *P* values were determined by Student *t* test or two-way ANOVA. *, $P < 0.05$; **, $P < 0.01$; ***, $P < 0.001$; ****, $P < 0.0001$.

Fig. S3A). Tumor growth in WT recipients receiving *mCd59ab*-deficient donor BM was significantly suppressed compared with that in those receiving WT donor BM (**Fig. 3A**-**C**). However, the tumor growth in *mCd59ab*-deficient recipients receiving WT donor BM displayed no difference from that in WT recipients transplanted with WT donor BM (**Fig. 3A**-**C**). In addition, tumors almost completely disappeared in *mCd59ab*-deficient recipients receiving *mCd59ab*-deficient donor BM (**Fig. 3A**-**C**). Thus, these results indicate that CD59

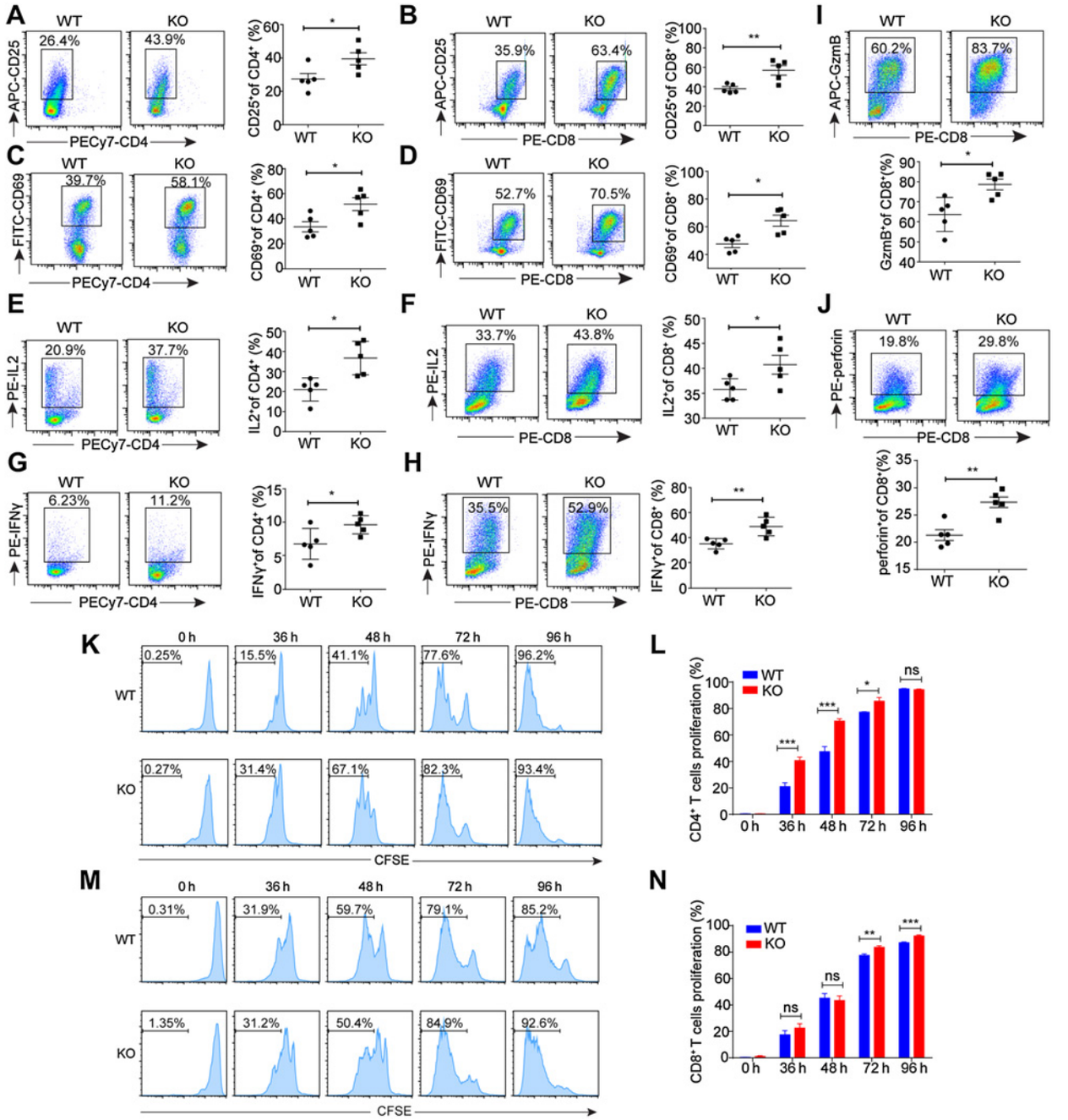

Figure 4.

mCd59ab deficiency enhances CD4$^+$ and CD8$^+$ T-cell activation and proliferation. **A–J,** Activation of naïve CD4$^+$ and CD8$^+$ T cells with or without *mCd59ab* deficiency. The expression of CD25 (**A, B**), CD69 (**C, D**), IL2 (**E, F**), IFNγ (**G, H**), granzyme B (**I**), and perforin (**J**) to evaluate T-cell activation by flow cytometry in naïve CD4$^+$ (**A, C, E,** and **G**) and CD8$^+$ (**B, D, F, H, I,** and **J**) T cells, which were isolated from the spleens of WT and *mCd59ab*$^{-/-}$ littermates using cell sorting. **K–N,** Naïve CD4$^+$ and CD8$^+$ T-cell division upon mIL2 and anti-CD3/CD28 treatment, as determined by CFSE staining at the indicated time in *mCd59ab*-WT or -KO cells. Representative flow cytometry images are shown in the left panel, and quantitative data are shown in the right panel. Data are expressed as the mean±SEM; $n = 5$. The *P* values were determined by Student *t* test. *, $P < 0.05$; **, $P < 0.01$; ***, $P < 0.001$; ns, not significant.

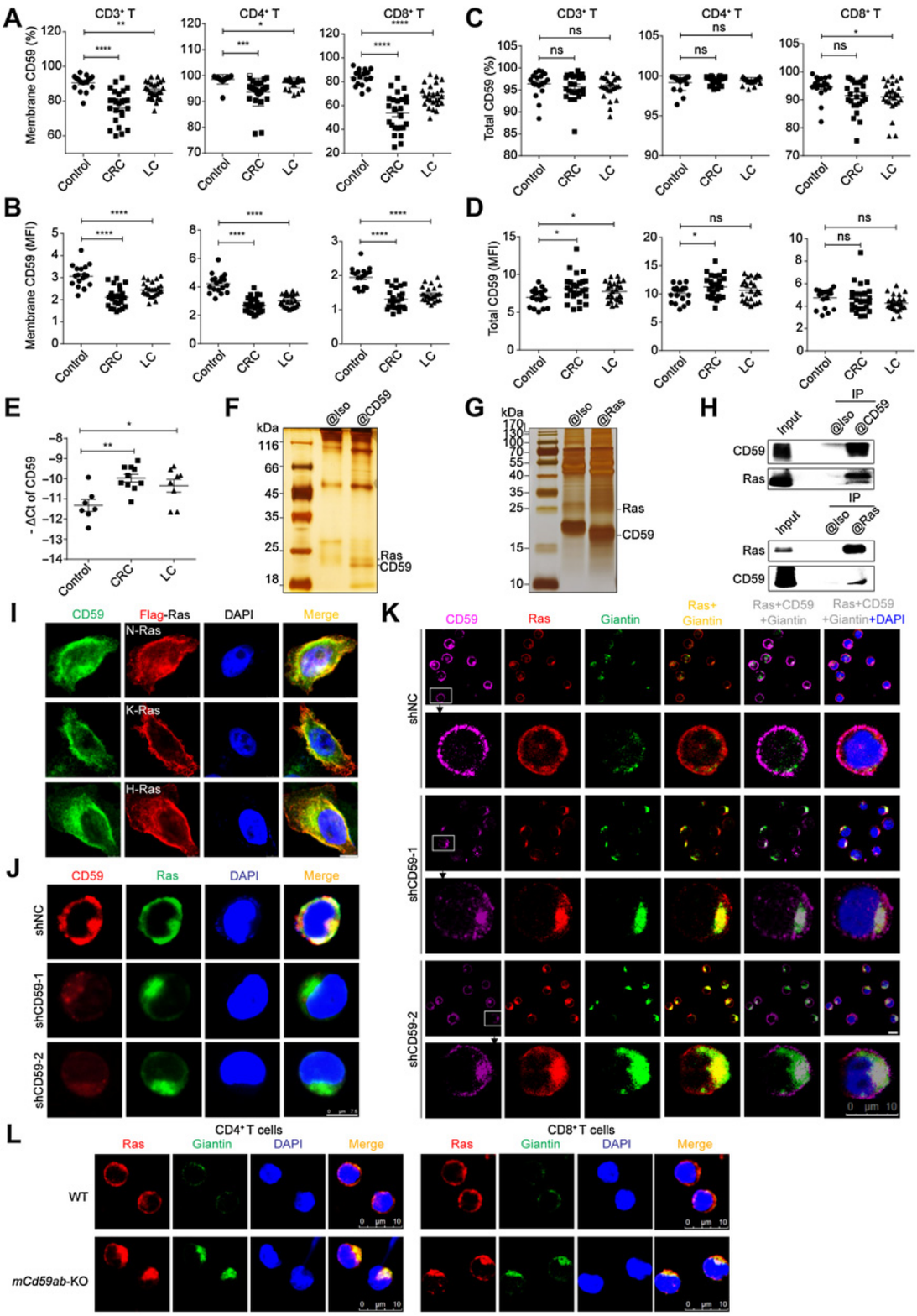
A
CD3+ T
CD4+ T
CD8+ T
Membrane CD59 (%)
Control
CRC
LC
B
Membrane CD59 (MFI)
C
Total CD59 (%)
ns
D
Total CD59 (MFI)
E
- ΔCt of CD59
F
kDa
@Iso
@CD59
Ras
CD59
G
@Ras
H
IP
Input
CD59
Ras
I
CD59
Flag-Ras
DAPI
Merge
N-Ras
K-Ras
H-Ras
J
shNC
shCD59-1
shCD59-2
K
Ras
Giantin
Ras+ Giantin
Ras+CD59 +Giantin
Ras+CD59 +Giantin+DAPI
L
CD4+ T cells
CD8+ T cells
WT
mCd59ab-KO

expression in immune cells is essential for regulating tumor cell proliferation.

Considering the fundamental roles of $CD4^+$ and $CD8^+$ T cells in the antitumor response, we next measured the proportions of these cell types in the blood of chimeric tumor-bearing mice. WT and *mCd59ab*-deficient mice receiving *mCd59ab*-deficient BM both exhibited higher $CD4^+$ (Supplementary Fig. S3B) and $CD8^+$ (Supplementary Fig. S3C) T-cell proportions in the blood than those receiving WT BM, suggesting that *mCd59ab* deficiency may promote T-cell development and/or proliferation in tumor-bearing mice.

To further validate whether $CD4^+$ and/or $CD8^+$ T cells are responsible for the tumor regression caused by *mCD59ab* deletion, we depleted $CD4^+$ or $CD8^+$ T cells or both by injecting specific mAbs into TC1 cell-implanted mice, with an anti-IgG isotype antibody used as a control (Supplementary Fig. S3D). The efficacy of T-cell depletion in the blood was confirmed at the endpoint of the experiment (Supplementary Fig. S3E–S3G). In WT mice, $CD8^+$ T-cell depletion slightly promoted tumor growth, whereas $CD4^+$ T-cell depletion instead impeded tumor growth (**Fig. 3D–F**; Supplementary Fig. S3H), which was in agreement with previous reports (32, 33). Depletion of both $CD4^+$ and $CD8^+$ T cells abolished the above effects of individual depletion of $CD4^+$ or $CD8^+$ T cells (**Fig. 3D–F**; Supplementary Fig. S3H). In *mCd59ab*-deficient mice, the depletion of $CD4^+$ T cells, $CD8^+$ T cells, and more potently both $CD4^+$ and $CD8^+$ T cells reversed the ability of *mCd59ab* deficiency to suppress tumors (**Fig. 3D–F**; Supplementary Fig. S3H). Together, these results demonstrate that $CD4^+$ T cells and, more potently, $CD8^+$ T cells are required for an effective antitumor response in *mCd59ab*-deficient mice.

CD59 deficiency enhances $CD4^+$ and $CD8^+$ T-cell activity and proliferation

Next, we sought to investigate the effect of CD59 deficiency on T-cell activation. Naïve $CD4^+$ and $CD8^+$ T cells were isolated from the spleens of WT and *mCd59ab*-deficient littermates and then stimulated with CD3/CD28 antibodies. At 24 h, the expression of CD25 and CD69, two T-cell activation markers, on $CD4^+$ and $CD8^+$ T showed that *mCd59ab*-deficient $CD4^+$ and $CD8^+$ T cells exhibited more active TCR signaling than WT $CD4^+$ and $CD8^+$ T cells (**Fig. 4A–D**). At 48 h, the above pretreated $CD4^+$ or $CD8^+$ T cells were further coincubated with PMA/ionomycin/BFA (PIB) for 4 to 6 h, showing that *mCd59ab* deficiency in $CD4^+$ and $CD8^+$ T cells significantly increased the expression of IL2 (**Fig. 4E** and **F**) and IFNγ (**Fig. 4G** and **H**). In addition, the expression of granzyme B (**Fig. 4I**) and perforin (**Fig. 4J**), the primary factors that mediate direct T-cell cytotoxicity, was also significantly elevated in *mCd59ab*-deficient $CD8^+$ T cells, indicating that their cytotoxic capability may be enhanced accordingly.

Furthermore, we detected the proliferation of $CD4^+$ and $CD8^+$ T cells from WT and *mCd59ab*-deficient mice. CFSE dilution analysis results revealed that upon anti-CD3/CD28 treatment, the division of *mCd59ab*-deficient $CD4^+$ or $CD8^+$ T cells was faster than that of their WT counterparts (**Fig. 4K–N**) and accompanied by higher expression of the intracellular proliferation-related nuclear antigen Ki-67 (Supplementary Fig. S4A and S4B).

In addition, we also analyzed the expressions of PD-1, CTLA4, TIM-3 and LAG3 in $CD3^+$, $CD4^+$ and $CD8^+$ T cells in the spleen of WT and *mCd59ab*$^{-/-}$ tumor-bearing mice. The results showed that there were no significant differences in the expressions of PD-1, CTLA4, TIM-3 and LAG3 in $CD3^+$ and $CD4^+$ T cells or PD-1, LAG3 in $CD8^+$ T cells between WT and *mCd59ab*-deficient mice, suggesting that the enhanced $CD3^+$ and $CD4^+$ T-cell activity resulted from CD59 deficiency may be not associated with these immunosuppressive molecules (Supplementary Fig. S5). However, the expression of CTLA4 and TIM-3 in $CD8^+$ T cells in the *mCd59ab*-deficient tumor-bearing mice were lower than those in the WT tumor-bearing mice, indicating that CTLA4 and TIM-3 might be involved in the regulation of $CD8^+$ T-cell activity by CD59 (Supplementary Fig. S5). Taken together, the results suggest that *mCd59ab* deficiency can significantly augment the activation, cytotoxicity and proliferation of $CD4^+$ and $CD8^+$ T cells *in vitro*.

Intracellular CD59 interacts with Ras proteins to switch Ras compartmentalization in the plasma membrane or Golgi

mCd59ab deficiency failed to change the immune cell count under physiologic conditions (Supplementary Fig. S1A and S1B) but instead increased the T-cell count in tumor-bearing mice (**Fig. 2**), suggesting that the complement-mediated function may not involve CD59 deficiency-induced tumor suppression. To further investigate CD59 function, using flow cytometry, we first detected the subcellular distribution of CD59 in blood $CD4^+$ and $CD8^+$ T cells of patients with healthy control, colorectal cancer, and lung cancer, specifically in membrane (without permeabilization) and in total (membrane + intracellular, with permeabilization). The surface CD59 abundance in $CD3^+$, $CD4^+$, and $CD8^+$ T cells of both patients with colorectal cancer and patients with lung cancer were significantly lower than those of healthy subjects, as determined by measuring the CD59-positive percentage (**Fig. 5A**) and mean fluorescence intensity (MFI; **Fig. 5B**). However, the total CD59 expression in patients with colorectal cancer and lung cancer was increased (the MFIs in $CD3^+$ T cells of patients with colorectal cancer and lung cancer and in $CD4^+$ T cells of patients with colorectal cancer) or remained unchanged (in other cell types) compared with that in healthy donors, except for the decrease observed in CD59-positive $CD8^+$ T cells in patients with lung cancer (**Fig. 5C** and **D**).We also performed qRT-PCR to detect mRNA expression of *CD59* in $CD3^+$ T cells of healthy donors and patients with cancer. The results showed that the mRNA abundance of *CD59* consistently elevated in patients with colorectal and lung cancer compared with that of healthy donors (**Fig. 5E**). These results indicate

Figure 5.

Intracellular CD59 regulates Ras subcellular compartmentalization in the plasma membrane or Golgi via a protein–protein interaction. **A–D,** Membrane (without permeabilization) and total (membrane + intracellular, with permeabilization) CD59 expression in T cells of healthy controls, patients with colorectal cancer and patients with lung cancer was detected by flow cytometry. The membrane (**A, B**) and total (**C, D**) CD59 expression displayed as the percentage of CD59-positive cells (**A, C**) and the MFI (**B, D**) in $CD3^+$, $CD4^+$, and $CD8^+$ T cells. Data are expressed as the mean±SEM; $n = 18$, healthy donor controls; $n = 26$, patients with colorectal cancer; $n = 25$, patients with lung cancer. The *P* values were determined by Student *t* test. *, $P < 0.05$; **, $P < 0.01$; ***, $P < 0.001$; ****, $P < 0.0001$; ns, not significant. **E,** The mRNA expressions of CD59 in $CD3^+$ T cells collected from healthy donors and patients with cancer were detected by qRT-PCR. $n = 7$, healthy donor controls; $n = 10$, patients with colorectal cancer; $n = 8$, patients with lung cancer. SDS-PAGE (**F–G**) and immunoblotting with co-IP and subsequent LC/MS-MS (**H**) using anti-CD59 and anti-Ras was used to identify CD59-Ras interactions in Jurkat T cells. Isotype IgG was used as a negative control in **F–H**. **I,** Endogenous CD59 and ectopic Flag-tagged N-, K-, or H-Ras in HeLa cells detected by ICC. **J,** shCD59-induced subcellular compartmentalization change of Ras in Jurkat T cells. **K,** Localization of CD59, Ras, and the Golgi in Jurkat T cells with shCD59 treatment, as detected by anti-Giantin. **L,** Subcellular localization of Ras in $CD4^+$ and $CD8^+$ T cells of WT and *mCd59ab*-KO mice. $n = 3$/group. Scale bar 7.5 μm (**I, J**) or 10 μm (**K, L**).

that in the T cells of patients with cancer, CD59 expression decreases on the cell membrane, thus possibly providing less protection from MAC attack, but increases intracellularly, thus playing a complement-independent role.

Reduced expression of GPI biosynthetic genes may lead to the decreased distribution of GPI anchored CD59 on the cell surface. It has been reported that membrane expression of CD59 is significantly reduced in cells with CRISPR-Cas9 knockout of GPI biosynthetic genes (*PIGA*/*PIGC*/*PIGH*/*PIGP*/*PIGQ*/*PIGY*/*PIGL*/*PIGW*/*PIGM*/*PIGX*/*PIGV*/*PIGN*/*PIGB*/*PIGO*/*PIGF*/*PIGK*/*PIGS*/*PIGT*/*PIGU*/*GPAA1*/*PGAP2*-KO cells; ref. 34). Therefore, we detected the expression of the above genes in T cells of healthy controls and patients with colorectal cancer and found that most of these genes (*PIGC*/*PIGH*/*PIGP*/*PIGQ*/*PIGY*/*PIGL*/*PIGW*/*PIGM*/*PIGX*/*PIGV*/*PIGN*/*PIGB*/*PIGO*/*PIGF*/*PIGK*/*PIGS*/*PIGT*/*PIGU*/*PGAP2*) were significantly decreased, and 2 genes (*PIGA* and *GPAA1*) were not significantly changed in patients with colorectal cancer compared with those in healthy controls (Supplementary Fig. S6). These results suggest that the reduced expression of the above genes possibly led to the decreased membrane expression of CD59, thus resulting in the accumulation of intracellular CD59 in T cells of patients with colorectal cancer.

On the basis of the above findings, we hypothesized that CD59 plays this complement-independent role inside T cells via a protein–protein interaction. Thus, using a CD59-specific antibody, we performed co-IP and LC/MS assays to identify CD59-binding proteins in Jurkat T cells (**Fig. 5F**, and Supplemental Data 3). Ras, a CD59-binding protein, was nominated for follow-up because: (i) a unique band around 20 kDa only existed in the anti-CD59 lane (**Fig. 5F**), and (ii) among four proteins around 20 kDa (CLCF1, IGLL5, ZAGL1, and NRAS, Supplemental Data 3), Ras/MAPK signaling has been reported crucial for T-cell development, proliferation, and function (5). Furthermore, using a Ras antibody, we performed a similar assay and verified that CD59 is a Ras-binding protein (**Fig. 5G**, and Supplemental Data 4). The interaction between CD59 and Ras was further confirmed in a mutual co-IP assay (**Fig. 5H**). Moreover, an immunocytochemistry (ICC) assay showed that all three Ras isoforms, N-, K-, and H-Ras, could interact with intracellular CD59 (**Fig. 5I**), indicating that the three Ras proteins bind to CD59 most likely via the N-terminal region. Therefore, these data established the interaction of Ras with CD59 inside T cells.

To further evaluate the intrinsic role of CD59 in regulating T-cell activation, we first established two CD59-insufficient Jurkat T-cell lines with distinct shRNAs, the efficacy (Supplementary Fig. S7A–S7C) and specificity (Supplementary Fig. S7D) of which were verified by RT-qPCR, immunoblotting and flow cytometry. In addition, ICC assay results further demonstrated the interaction of CD59 with Ras in Jurkat T cells, as this interaction was remarkably weakened by CD59 insufficiency (**Fig. 5J**). Thus, these results further support that CD59 likely regulates T-cell activation via an interaction with Ras.

In the above ICC assay, more importantly, we found that the diffuse distribution of Ras changed to accumulation in a certain subcellular site upon CD59 insufficiency (**Fig. 5J**). It has been reported that growth factor-induced Ras signaling activation on the plasma membrane is rapid and transient, whereas Ras signaling in the Golgi is delayed and sustained (11, 12, 35). Furthermore, if Jurkat T cells are treated with low-grade TCR stimulation, N-Ras activation occurs entirely at the Golgi in a PLCγ- and RasGRP1-dependent manner (6). Thus, using a specific antibody against Giantin, a Golgi marker, we performed an ICC assay to evaluate Ras subcellular localization. In CD59-sufficient cells, almost all Ras protein was distributed in the plasma membrane, with little localized in the Golgi. In contrast, in CD59-insufficient cells, almost all Ras protein was restricted in the Golgi, with little localized in the plasma membrane (**Fig. 5K**), and a similar behavior of Ras subcellular distribution in $CD4^+$ and $CD8^+$ T cells was observed in *mCd59ab*$^{-/-}$ mice (**Fig. 5L**). Therefore, these results indicate that upon CD59 insufficiency, Ras is predominantly retained in the Golgi in the transport process, potentially inducing delayed and sustained signaling (6, 11, 12, 35).

CD59 regulates T-cell activation via the MAPK pathway

Furthermore, we explored the function of CD59 insufficiency in Jurkat T-cell activation and observed that CD59 insufficiency could significantly enhance the expression of CD69 (**Fig. 6A** and **B**) and IL2 (**Fig. 6C**) upon stimulation with anti-CD3/CD28 or additional PIB, consistent with the data from *mCd59ab*-deficient mice.

Upon TCR engagement during T-cell activation, many signaling pathways are involved in downstream processes, including the MAPK, PI3K/AKT, and NF-κB pathways, which result in cellular activation, development, proliferation, and gene induction. MAPKs are the main Ras-regulated downstream molecules and are grouped into three major families: ERKs, p38, and JNKs. ERKs are mainly activated by MEK1 and MEK2; p38 is activated by MKK3, MKK4, and MKK6; and JNKs are activated by MKK4 and MKK7. Thus, we compared the activation of MAPK signaling in CD59-sufficient and CD59-insufficient Jurkat T cells. The results demonstrated that the phosphorylation of MEK1/2, ERK1/2, MKK3/MKK6, p38, MKK4, and JNK was enhanced by anti-CD3/CD28 in CD59-insufficient cells compared with CD59-sufficient cells (**Fig. 6D**). These results were further confirmed by flow cytometry, which showed that p-ERK1/2, p-p38, and p-JNK were elevated in CD59-insufficient Jurkat T cells (**Fig. 6E**). In addition, we knocked down the expression of N-Ras, K-Ras, and H-Ras in CD59-insufficient Jurkat T cells and then detected the activation of downstream signaling of Ras. The result demonstrated that the deficiency of Ras could reduce phosphorylation of ERK1/2, p38, and JNK induced by CD59 insufficiency, which indicated that the increased MAPK signaling activation in CD59-deficient cells depends on the interaction of CD59 with Ras proteins (Supplementary Fig. S8A). Moreover, when Jurkat T cells were pretreated with the MEK1/2 kinase-specific inhibitor U0126, p38 kinase inhibitor SB203580, or JNK kinase inhibitor JNKIN8 prior to anti-CD3/CD28 stimulation, CD59 insufficiency-enhanced T-cell activation was almost completely abrogated, as determined by the dramatic decreases in the expression of CD69 and IL2 to that of CD59-sufficient cells (Supplementary Fig. S8B–S8D). These *in vitro* results indicate that CD59 insufficiency activates the MAPK pathway to enhance T-cell activation.

To confirm that MAPK activation in T cells is induced by CD59 deficiency *in vivo*, we collected splenic $CD4^+$ and $CD8^+$ T cells from the above WT and *mCd59ab*-deficient tumor-bearing littermates. Flow cytometric analysis showed higher proportions of p-ERK-, p-p38-, and p-JNK–positive $CD4^+$ (**Fig. 6F**) and $CD8^+$ T (**Fig. 6G**) cells in the *mCd59ab*-deficient mice than in the WT mice. Taken together, these findings strongly suggest that T-cell activation can be enhanced by reducing CD59 expression and the resultant MAPK activation.

CD59 insufficiency activates MAPK signaling and enhances human T-cell function

To confirm the regulatory effect of CD59 on normal human T cells from healthy donors, we separately induced CD59 insufficiency with two specific shRNAs, for which the knockdown efficacy was

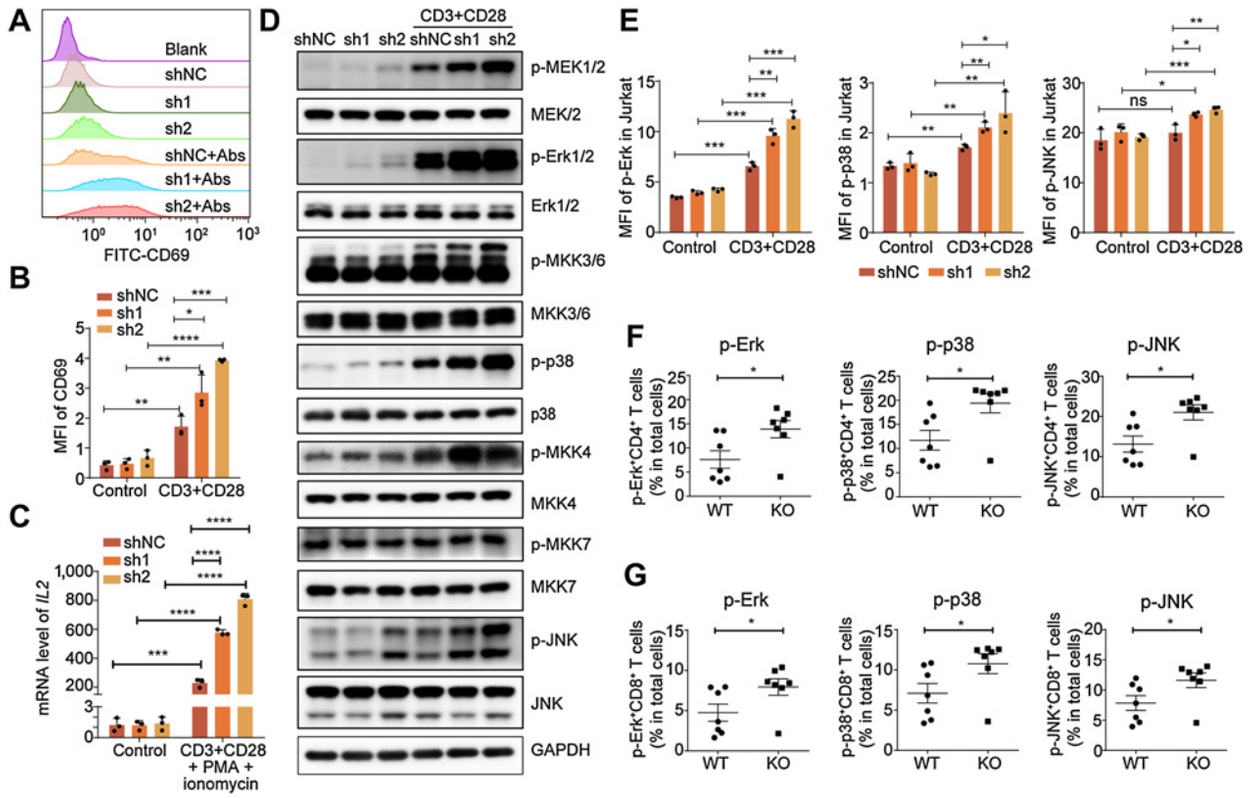

Figure 6.

CD59 insufficiency enhanced Jurkat T-cell activation via MAPK signaling. **A–C,** A flow cytometry assay was employed to detect CD69 upon anti-CD3/CD28 treatment (**A**), and the quantitative results are shown in (**B**). A qRT-PCR assay was used to detect IL2 transcription after additional treatment with PMA and ionomycin (**C**). **D,** Immunoblotting assay of components of three MAPK signaling pathways in Jurkat T cells with CD59 insufficiency. **E,** Phosphorylation of ERK, p38, and JNK in Jurkat T cells with CD59 insufficiency, as measured by flow cytometry. Data are expressed as the mean±SD. Control: shNC, shCD59–1: sh1, shCD59–2: sh2. The experiments were performed in triplicate. (**F–G**) Phosphorylation of ERK, p38, and JNK in T cells of *mCd59ab*-deficient tumor-bearing mice. $CD4^+$ (**F**) and $CD8^+$ (**G**) T cells were isolated from the spleens of TC-1 tumor-bearing WT or *mCD59ab*$^{-/-}$ littermates. Data are expressed as the mean±SEM. $n = 7$/group. The *P* values were determined by Student *t* test. *, $P < 0.05$; **, $P < 0.01$; ***, $P < 0.001$; ns, not significant.

determined by flow cytometry (Supplementary Fig. S7E). Upon anti-CD3/CD28 treatment, the expression of TNFα (**Fig. 7A**) and IFNγ (**Fig. 7B**) increased significantly, as detected by flow cytometry at both 24 hours and 48 hours. However, in contrast to our *in vitro* results, CD59 insufficiency failed to increase IL2 expression (**Fig. 7C**). Furthermore, we detected the activation of MAPK signaling and found that CD59 insufficiency significantly enhanced the phosphorylation of ERK, p38, and JNK, especially upon anti-CD3/CD28 treatment (**Fig. 7D** and **E**). Therefore, these results demonstrated that in normal human T cells, reducing CD59 expression could also enhance MAPK signaling activation, thus upregulating T-cell activation, as indicated by the increases in the expression of effector molecules including TNFα and IFNγ.

Discussion

T lymphocytes play an essential role in cancer immunotherapy; however, the current strategies targeting T cells, including anti-CTLA4 and anti–PD-1/PD-L1, have achieved satisfactory clinical responses in only 20% to 40% of patients with cancer (1). Therefore, it is necessary to better understand T-cell activation signaling to design future T cell–targeted therapeutics. In the current study, we provide another strategy for T-cell activation. Intracellular CD59 regulates the RAS/MAPK pathway through an interaction with Ras and results in a Ras subcellular switch in the plasma membrane or Golgi, thus modulating the downstream MAPK signaling of Ras and ultimately regulating T-cell activation (**Fig. 7F**).

Numerous studies have revealed the complement-dependent roles of CD59 in tumor progression and drug resistance but have mainly focused on membrane-bound CD59 in tumor cells (36). However, there are few studies on intracellular CD59. In patients with cancer, we found that membrane-bound CD59 was decreased, and intracellular CD59 was increased in both $CD4^+$ T cells and $CD8^+$ T cells. Using *mCd59ab*-deficient mice, we revealed that *mCd59ab* deficiency almost completely abrogated tumor growth and metastasis by potently enhancing $CD4^+$ and especially $CD8^+$ T-cell function and proliferation. Considering that the classic function of CD59 is to block the assembly of the complement MAC in the cell membrane, we revealed that CD59 inside T cells might play a complement-independent role. Furthermore, we reported that in Jurkat T cells, CD59 interacts with Ras, a key signaling molecule in T-cell activation, and that the abundance of CD59 may change the subcellular location of Ras for T-cell

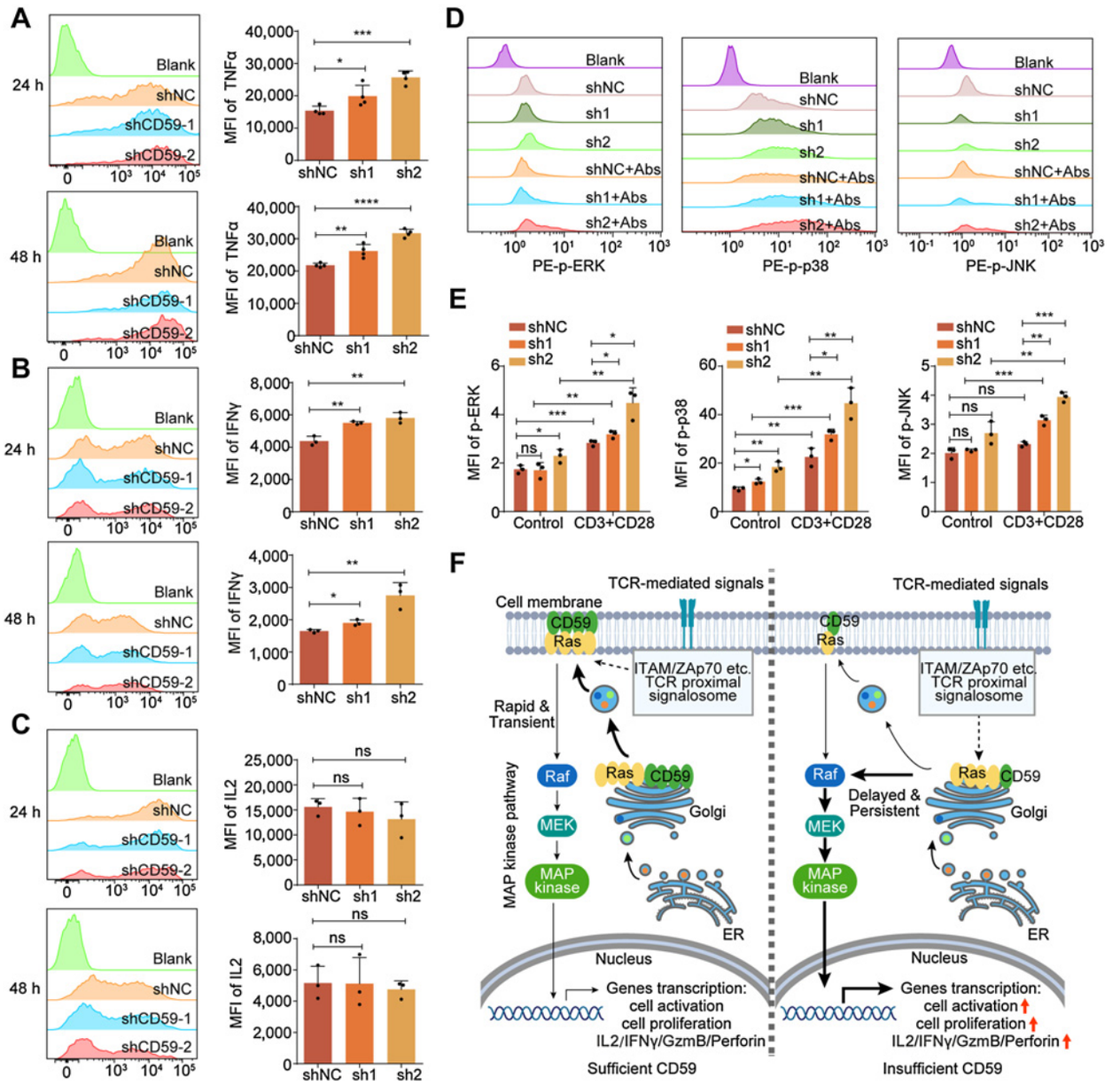

Figure 7.

CD59 insufficiency enhanced human T-cell effector function via the MAPK pathway. **A–C,** The effect of CD59 insufficiency on human T-cell function upon treatment with IL2, anti-CD3/CD28, and additional PMA/ionomycin/BFA. The expression of TNFα (**A**), IFNγ (**B**), and IL2 (**C**) was detected by flow cytometry. **D** and **E,** Phosphorylation of MAPK signaling components in CD59-insufficient human T cells following the same treatment. Phosphorylation of ERK, p38, and JNK was detected by flow cytometry (**D**), and the quantitative results are shown in (**E**). Images are representative of three or four independent experiments. The *P* values were determined by Student *t* test. *, $P < 0.05$; **, $P < 0.01$; ***, $P < 0.001$; ns, not significant. **F,** Schematic diagram of the regulatory effect of the CD59 interaction with Ras on T cells. A high CD59 abundance facilitates Ras transportation to the inner plasma membrane, thus leading to rapid and transient activation of the Ras/Raf/MEK/MAPK pathway and limited T-cell activation and proliferation, whereas low or null CD59 changes the subcellular compartmentalization of Ras to the Golgi, thus leading to delayed and persistent Ras/Raf/MEK/MAPK signaling and resultant enhanced T-cell activation and proliferation.

activation. When CD59 is abundant, it facilitates Ras transport to the T-cell inner plasma membrane via a protein–protein interaction, resulting in membrane Ras inducing rapid and transient signaling; in contrast, when CD59 is insufficient or deficient, Ras membrane transport is suppressed, and Ras is retained in the Golgi, thus generating delayed and persistent signaling (6, 11, 12, 35), which further enhances downstream MAPK signaling (ref. 9; **Fig. 7F**). Thus, we observed that CD59 deficiency or insufficiency potently enhanced T-cell activation, proliferation, and function by activating MAPK signaling.

Subcellular compartmentalization, such as that shown for Ras, provides spatial selectivity for increasing the signal complexity of

individual molecular cascades (13). This spatial regulation of Ras signaling can also lead to different biological functions. In T lymphocytes, TCR signaling induces Ras activation specifically in the Golgi, leading to cell growth; however, the combination of LFA-1 and TCR signaling results in Ras activation in the plasma membrane, promoting cell adhesion (13, 37, 38). In epithelial cells, two Golgi-specific transmembrane proteins, PAQR10 and PAQR11, may increase Ras Golgi retention via interactions with Ras, thus enhancing ERK signaling (39).

MAPKs are involved in many physiologic processes in T cells, including development, homeostasis, and proliferation. In this study, we demonstrated that insufficiency or deficiency in CD59 enhanced the T-cell immune response by activating the Ras/MAPK signaling pathway, which was initiated by the activation of Ras in the Golgi. Consistently, a significant pool of N-Ras and H-Ras resides in the Golgi (40, 41).

The association between CD59 deficiency/defect and abnormal T-cell responses has been implied mainly in paroxysmal nocturnal hemoglobinuria (PNH) and inherited CD59 deficiency disease. PNH is an acquired rare disease with the phosphatidylinositol glycan-class A (*PIGA*) gene mutation in hematopoietic stem cell, which results in the membrane loss of GPI-anchored proteins, including complement-regulatory membrane proteins CD55 and CD59 (42). Though the PNH clones may be destroyed by excessive complement activation, they still acquire the expansion and survival advantage through unknown mechanisms. *PIGA* gene mutations alone do not explain this advantage of PNH clones, and abnormal T lymphocytes expand in many patients with PNH that may be involved in the pathogenesis of PNH (43, 44). Moreover, immunosuppressive therapy (antithymocyte globulin plus cyclosporin) is effective in some patients with PNH, and the PNH clone predicted a fast response to immunosuppressive therapy in patients with severe aplastic anemia (45, 46). In a MRL/lpr systemic lupus erythematosus murine model, mouse CD59a deficiency significantly exacerbated a number of autoimmune disease features, including increased weights of spleen and lymph node, lymphoproliferation, dermatitis, autoantibody production, and nephritis, which was independent of complement function (47). In addition, inherited CD59 deficiency is a rare autosomal recessive disorder characterized by chronic hemolysis, recurrent ischemic central nervous system strokes, and early-onset recurrent peripheral neuropathy resembling Guillain–Barré syndrome or chronic inflammatory demyelinating polyneuropathy. These patients harbor homozygous missense (p.Cys89Tyr, p.Asp49Val or c.A146T) or a frameshift deletion (c.146delA, p.Asp49Valfs*31) mutations in *CD59*. These mutations lead to membrane expression loss of CD59, but not CD55, on erythrocytes, monocytes, lymphocytes, and sural nerve (48, 49). Loss of membrane CD59 makes cells susceptible to complement-driven cytolysis, thus resulting in chronic hemolysis and possible nervous system injury; therefore, hemolysis is quickly controlled by the first infusion with eculizumab, a complement C5-targeted antibody, but an infant case demonstrated detectable improvement of neurologic status only about 6 months after the first treatment (50). Eculizumab treatment after 24 months also led to neurologic recovery, especially in the upper limbs and trunk in 4 patients (51). These clinical outcomes suggest that other complement-independent mechanism may be involved in the pathogenesis of inherited CD59 deficiency due to the slow and partial response of neurologic disorder to eculizumab treatment. Considering the central role of T lymphocytes in adaptive immunity and autoimmune diseases, including neural cell demyelinating damage (52, 53), these findings imply that decreased expression and/or intracellular accumulation of CD59 in T cells might play a distinct role in regulating the T lymphocyte–mediated diseases via complement-independent mechanisms, such as the interaction with Ras.

Immune cells other than T cells are also associated with tumor progression. MDSCs are immunosuppressive precursors of dendritic cells, macrophages, and granulocytes. MDSCs can promote tumor angiogenesis and disrupt immune surveillance by interfering with antigen presentation by DCs, T-cell activation, and NK cell–mediated cytotoxicity (54). Although neutrophils may be protective, particularly in antibody-mediated immunotherapy, they are widely recognized to promote tumor progression by multiple processes, including acting as MDSCs (55). Here, we observed that the proportions of MDSCs, neutrophils and macrophages were decreased significantly in CD59-deficient tumor-bearing mice compared with WT tumor-bearing mice. Although the depletion of $CD4^+$ T cells and especially $CD8^+$ T cells almost completely abolished the inhibitory effect of *mCd59ab* deficiency on tumor growth, the involvement of other immune cells, such as MDSCs and neutrophils, requires future investigation.

In summary, we identified a novel Ras regulator for Ras/MAPK signaling activation in the T-cell immune response. In the context of CD59 insufficiency or deficiency, Ras can be arrested in the Golgi, preventing transport to the plasma membrane, via an interaction with abundant CD59, thus inducing delayed and persistent MAPK activation and a resultant strong antitumor T-cell response. These results also suggest that CD59 may be a potential drug target for tumor immunotherapy.

Authors' Disclosures

No disclosures were reported.

Authors' Contributions

L. Li: Conceptualization, data curation, software, formal analysis, validation, investigation, visualization, methodology, writing–original draft, writing–review and editing. **P. Ding:** Software, formal analysis, supervision, validation, investigation, methodology. **X. Lv:** Software, formal analysis, supervision, validation, investigation, methodology. **S. Xie:** Resources, methodology. **L. Li:** Resources, formal analysis, supervision, investigation, methodology. **J. Chen:** Software, formal analysis, supervision, investigation, methodology. **D. Zhou:** Methodology. **X. Wang:** Methodology. **Q. Wang:** Software, methodology. **W. Zhang:** Software, methodology. **Y. Xu:** Methodology. **R. Lu:** Resources, methodology. **W. Hu:** Conceptualization, resources, data curation, formal analysis, supervision, funding acquisition, validation, investigation, visualization, methodology, writing–original draft, project administration, writing–review and editing.

Acknowledgments

This work was supported by grants to W. Hu from the National Natural Science Foundation of China (81790254, 81872354, and 82121004).

The publication costs of this article were defrayed in part by the payment of publication fees. Therefore, and solely to indicate this fact, this article is hereby marked "advertisement" in accordance with 18 USC section 1734.

Note

Supplementary data for this article are available at Cancer Immunology Research Online (http://cancerimmunolres.aacrjournals.org/).

Received December 15, 2021; revised July 27, 2022; accepted September 30, 2022; published first October 7, 2022.

Reference

1. Sharma P, Allison JP. The future of immune checkpoint therapy. Science 2015; 348:56–61.
2. Linsley PS, Greene JL, Brady W, Bajorath J, Ledbetter JA, Peach R. Human B7–1 (CD80) and B7–2 (CD86) bind with similar avidities but distinct kinetics to CD28 and CTLA4 receptors. Immunity 1994;1:793–801.
3. Yokosuka T, Takamatsu M, Kobayashi-Imanishi W, Hashimoto-Tane A, Azuma M, Saito T. Programmed cell death 1 forms negative costimulatory microclusters that directly inhibit T-cell receptor signaling by recruiting phosphatase SHP2. J Exp Med 2012;209:1201–17.
4. Sadelain M, Riviere I, Riddell S. Therapeutic T cell engineering. Nature 2017;545: 423–31.
5. Kortum RL, Rouquette-Jazdanian AK, Samelson LE. Ras and extracellular signal-regulated kinase signaling in thymocytes and T cells. Trends Immunol 2013;34:259–68.
6. Perez de Castro I, Bivona TG, Philips MR, Pellicer A. Ras activation in Jurkat T cells following low-grade stimulation of the T-cell receptor is specific to N-Ras and occurs only on the Golgi apparatus. Mol Cell Biol 2004;24:3485–963496.
7. Fehrenbacher N, Bar-Sagi D, Philips M. Ras/MAPK signaling from endomembranes. Molecular oncology 2009;3:297–307.
8. Caloca MJ, Zugaza JL, Bustelo XR. Exchange factors of the RasGRP family mediate Ras activation in the Golgi. J Biol Chem 2003;278:33465–73.
9. Bivona TG, Perez De Castro I, Ahearn IM, Grana TM, Chiu VK, Lockyer PJ, et al. Phospholipase Cgamma activates Ras on the Golgi apparatus by means of RasGRP1. Nature 2003;424:694–8.
10. Arozarena I, Matallanas D, Berciano MT, Sanz-Moreno V, Calvo F, Munoz MT, et al. Activation of H-Ras in the endoplasmic reticulum by the RasGRF family guanine nucleotide exchange factors. Mol Cell Biol 2004;24:1516–30.
11. Chiu VK, Bivona T, Hach A, Sajous JB, Silletti J, Wiener H, et al. Ras signaling on the endoplasmic reticulum and the Golgi. Nat Cell Biol 2002;4:343–50.
12. Rocks O, Peyker A, Kahms M, Verveer PJ, Koerner C, Lumbierres M, et al. An acylation cycle regulates localization and activity of palmitoylated Ras isoforms. Science 2005;307:1746–52.
13. Mor A, Philips MR. Compartmentalized Ras/MAPK signaling. Annu Rev Immunol 2006;24:771–800.
14. Morgan BP. Complement membrane attack on nucleated cells: resistance, recovery, and nonlethal effects. Biochem J 1989;264:1–14.
15. Chen J, Ding P, Li L, Gu H, Zhang X, Zhang L, et al. CD59 regulation by SOX2 is required for epithelial cancer stem cells to evade complement surveillance. Stem Cell Reports 2017;8:140–51.
16. Kesselring R, Thiel A, Pries R, Fichtner-Feigl S, Brunner S, Seidel P, et al. The complement receptors CD46, CD55 and CD59 are regulated by the tumor microenvironment of head and neck cancer to facilitate escape of complement attack. Eur J Cancer 2014;50:2152–61.
17. Zhou Y, Chu L, Wang Q, Dai W, Zhang X, Chen J, et al. CD59 is a potential biomarker of esophageal squamous cell carcinoma radioresistance by affecting DNA repair. Cell Death Dis 2018;9:887.
18. Krus U, King BC, Nagaraj V, Gandasi NR, Sjolander J, Buda P, et al. The complement inhibitor CD59 regulates insulin secretion by modulating exocytotic events. Cell Metab 2014;19:883–90.
19. Golec E, Rosberg R, Zhang E, Renstrom E, Blom AM, King BC. A cryptic non–GPI-anchored cytosolic isoform of CD59 controls insulin exocytosis in pancreatic β cells by interaction with SNARE proteins. FASEB J 2019;33:12425–34.
20. Golec E, Ekstrom A, Noga M, Omar-Hmeadi M, Lund PE, Villoutreix BO, et al. Alternative splicing encodes functional intracellular CD59 isoforms that mediate insulin secretion and are downregulated in diabetic islets. Proc Natl Acad Sci U S A 2022;119:e2120083119.
21. Korty PE, Brando C, Shevach EM. CD59 functions as a signal-transducing molecule for human T-cell activation. J Immunol 1991;146:4092–8.
22. Deckert M, Kubar J, Zoccola D, Bernard-Pomier G, Angelisova P, Horejsi V, et al. CD59 molecule: a second ligand for CD2 in T-cell adhesion. Eur J Immunol 1992; 22:2943–7.
23. Hahn WC, Menu E, Bothwell AL, Sims PJ, Bierer BE. Overlapping but non-identical binding sites on CD2 for CD58 and a second ligand CD59. Science 1992; 256:1805–7.
24. Arulanandam AR, Moingeon P, Concino MF, Recny MA, Kato K, Yagita H, et al. A soluble multimeric recombinant CD2 protein identifies CD48 as a low affinity ligand for human CD2: divergence of CD2 ligands during the evolution of humans and mice. J Exp Med 1993;177:1439–50.
25. Menu E, Tsai BC, Bothwell AL, Sims PJ, Bierer BE. CD59 costimulation of T-cell activation. CD58 dependence and requirement for glycosylation. J Immunol 1994;153:2444–56.
26. Longhi MP, Sivasankar B, Omidvar N, Morgan BP, Gallimore A. Cutting edge: murine CD59a modulates antiviral $CD4^+$ T cell activity in a complement-independent manner. J Immunol 2005;175:7098–102.
27. Sivasankar B, Longhi MP, Gallagher KM, Betts GJ, Morgan BP, Godkin AJ, et al. CD59 blockade enhances antigen-specific $CD4^+$ T cell responses in humans: a new target for cancer immunotherapy? J Immunol 2009;182: 5203–7.
28. Xie XH, Gao MH, Zhang B, Wang MJ, Wang J. Post-transcriptional CD59 gene silencing by siRNAs induces enhanced human T-lymphocyte response to tumor cell lysate-loaded DCs. Cell Immunol 2012;274:1–11.
29. Lipp AM, Juhasz K, Paar C, Ogris C, Eckerstorfer P, Thuenauer R, et al. Lck mediates signal transmission from CD59 to the TCR/CD3 pathway in Jurkat T cells. PLoS One 2014;9:e85934.
30. Qin X, Hu W, Song W, Grubissich L, Hu X, Wu G, et al. Generation and phenotyping of mCd59a and mCd59b double-knockout mice. Am J Hematol 2009;84:65–70.
31. Tang X, Kuhlenschmidt TB, Li Q, Ali S, Lezmi S, Chen H, et al. A mechanically induced colon cancer cell population shows increased metastatic potential. Mol Cancer 2014;13:131.
32. Ueha S, Yokochi S, Ishiwata Y, Ogiwara H, Chand K, Nakajima T, et al. Robust antitumor effects of combined anti–CD4-depleting antibody and anti–PD-1/PD-L1 immune checkpoint antibody treatment in mice. Cancer Immunol Res 2015;3:631–40.
33. Zha H, Wang X, Zhu Y, Chen D, Han X, Yang F, et al. Intracellular activation of complement C3 leads to PD-L1 antibody treatment resistance by modulating tumor-associated macrophages. Cancer Immunol Res 2019; 7:193–207.
34. Liu SS, Liu YS, Guo XY, Murakami Y, Yang G, Gao XD, et al. A knockout cell library of GPI biosynthetic genes for functional studies of GPI-anchored proteins. Commun Biol 2021;4:777.
35. Peyker A, Rocks O, Bastiaens PI. Imaging activation of two Ras isoforms simultaneously in a single cell. Chembiochem 2005;6:78–85.
36. Zhang R, Liu Q, Liao Q, Zhao Y. CD59: a promising target for tumor immunotherapy. Future Oncol 2018;14:781–91.
37. Mor A, Dustin ML, Philips MR. Small GTPases and LFA-1 reciprocally modulate adhesion and signaling. Immunol Rev 2007;218:114–25.
38. Mor A, Campi G, Du G, Zheng Y, Foster DA, Dustin ML, et al. The lymphocyte function-associated antigen-1 receptor costimulates plasma membrane Ras via phospholipase D2. Nat Cell Biol 2007;9:713–9.
39. Jin T, Ding Q, Huang H, Xu D, Jiang Y, Zhou B, et al. PAQR10 and PAQR11 mediate Ras signaling in the Golgi apparatus. Cell Res 2012;22: 661–76.
40. Choy E, Chiu VK, Silletti J, Feoktistov M, Morimoto T, Michaelson D, et al. Endomembrane trafficking of Ras: the CAAX motif targets proteins to the ER and Golgi. Cell 1999;98:69–80.
41. Apolloni A, Prior IA, Lindsay M, Parton RG, Hancock JF. H-ras but not K-Ras traffics to the plasma membrane through the exocytic pathway. Mol Cell Biol 2000;20:2475–87.
42. Takeda J, Miyata T, Kawagoe K, Iida Y, Endo Y, Fujita T, et al. Deficiency of the GPI anchor caused by a somatic mutation of the PIG-A gene in paroxysmal nocturnal hemoglobinuria. Cell 1993;73:703–11.
43. Murakami Y, Kinoshita T, Maeda Y, Nakano T, Kosaka H, Takeda J. Different roles of glycosylphosphatidylinositol in various hematopoietic cells as revealed by a mouse model of paroxysmal nocturnal hemoglobinuria. Blood 1999;94: 2963–70.
44. Visconte V, Raghavachari N, Liu D, Keyvanfar K, Desierto MJ, Chen J, et al. Phenotypic and functional characterization of a mouse model of targeted PIG-A deletion in hematopoietic cells. Haematologica 2010;95: 214–23.
45. Ren X, Li X, Huo J, You Y, Huang J, Shao Y, et al. Small PNH clones detected by fluorescent aerolysin predict a faster response to immunosuppressive therapy in patients with severe aplastic anemia. Hematology 2020;25:348–55.
46. Sugimori C, Chuhjo T, Feng X, Yamazaki H, Takami A, Teramura M, et al. Minor population of CD55-CD59- blood cells predicts response to immunosuppressive therapy and prognosis in patients with aplastic anemia. Blood 2006;107:1308–14.

47. Miwa T, Zhou L, Maldonado MA, Madaio MP, Eisenberg RA, Song WC. Absence of CD59 exacerbates systemic autoimmunity in MRL/lpr mice. J Immunol 2012;189:5434–41.
48. Nevo Y, Ben-Zeev B, Tabib A, Straussberg R, Anikster Y, Shorer Z, et al. CD59 deficiency is associated with chronic hemolysis and childhood relapsing immune-mediated polyneuropathy. Blood 2013;121:129–35.
49. Haliloglu G, Maluenda J, Sayinbatur B, Aumont C, Temucin C, Tavil B, et al. Early-onset chronic axonal neuropathy, strokes, and hemolysis: inherited CD59 deficiency. Neurology 2015;84:1220–4.
50. Höchsmann B, Dohna-Schwake C, Kyrieleis HA, Pannicke U, Schrezenmeier H. Targeted therapy with eculizumab for inherited CD59 deficiency. N Engl J Med 2014;370:90–2.
51. Mevorach D, Reiner I, Grau A, Ilan U, Berkun Y, Ta-Shma A, et al. Therapy with eculizumab for patients with CD59 p.Cys89Tyr mutation. Ann Neurol 2016;80:708–17.
52. Khan U, Ghazanfar H. T Lymphocytes and Autoimmunity. Int Rev Cell Mol Biol 2018;341:125–68.
53. Feng D, Dai S, Liu F, Ohtake Y, Zhou Z, Wang H, et al. Cre-inducible human CD59 mediates rapid cell ablation after intermedilysin administration. J Clin Invest 2016;126:2321–33.
54. Gabrilovich DI. Myeloid-derived suppressor cells. Cancer Immunol Res 2017;5:3–8.
55. Treffers LW, Hiemstra IH, Kuijpers TW, van den Berg TK, Matlung HL. Neutrophils in cancer. Immunol Rev 2016;273:312–28.